Editors' Suggestion
Featured in Physics

# Measurement of the Cosmic Ray Helium Energy Spectrum from 70 GeV to 80 TeV with the DAMPE Space Mission

F. Alemanno,[1,2] Q. An,[3,4] P. Azzarello,[5] F. C. T. Barbato,[1,2] P. Bernardini,[6,7] X. J. Bi,[8,9] M. S. Cai,[10,11] E. Catanzani,[12] J. Chang,[10,11] D. Y. Chen,[9,10] J. L. Chen,[13] Z. F. Chen,[10,11] M. Y. Cui,[10] T. S. Cui,[14] Y. X. Cui,[10,11] H. T. Dai,[3,4] A. D'Amone,[6,7] A. De Benedittis,[6,7] I. De Mitri,[1,2] F. de Palma,[6,7] M. Deliyergiyev,[5] M. Di Santo,[6,7,*] T. K. Dong,[10] Z. X. Dong,[14] G. Donvito,[15] D. Droz,[5] J. L. Duan,[13] K. K. Duan,[10] D. D'Urso,[12,†] R. R. Fan,[8] Y. Z. Fan,[10,11] K. Fang,[8] F. Fang,[13] C. Q. Feng,[3,4] L. Feng,[10] P. Fusco,[15,16] M. Gao,[8] F. Gargano,[15] K. Gong,[8] Y. Z. Gong,[10] D. Y. Guo,[8] J. H. Guo,[10,11] X. L. Guo,[10,11] S. X. Han,[14] Y. M. Hu,[10] G. S. Huang,[3,4] X. Y. Huang,[10,11] Y. Y. Huang,[10] M. Ionica,[12] W. Jiang,[10,11] J. Kong,[13] A. Kotenko,[5] D. Kyratzis,[1,2] S. J. Lei,[10] S. Li,[10] W. L. Li,[14] X. Li,[10] X. Q. Li,[14] Y. M. Liang,[14] C. M. Liu,[3,4] H. Liu,[10] J. Liu,[13] S. B. Liu,[3,4] W. Q. Liu,[13] Y. Liu,[10] F. Loparco,[15,16] C. N. Luo,[10,11] M. Ma,[14] P. X. Ma,[10] T. Ma,[10] X. Y. Ma,[14] G. Marsella,[6,7,‡] M. N. Mazziotta,[15] D. Mo,[13] X. Y. Niu,[13] X. Pan,[10,11] A. Parenti,[1,2] W. X. Peng,[8] X. Y. Peng,[10] C. Perrina,[5,§] R. Qiao,[8] J. N. Rao,[14] A. Ruina,[5] M. M. Salinas,[5] G. Z. Shang,[14] W. H. Shen,[14] Z. Q. Shen,[10] Z. T. Shen,[3,4] L. Silveri,[1,2] J. X. Song,[14] M. Stolpovskiy,[5] H. Su,[13] M. Su,[17] Z. Y. Sun,[13] A. Surdo,[7] X. J. Teng,[14] A. Tykhonov,[5] H. Wang,[14] J. Z. Wang,[8] L. G. Wang,[14] S. Wang,[10,11] X. L. Wang,[3,4] Y. Wang,[3,4] Y. F. Wang,[3,4] Y. Z. Wang,[10] Z. M. Wang,[1,2,‖] D. M. Wei,[10,11] J. J. Wei,[10] Y. F. Wei,[3,4] S. C. Wen,[3,4] D. Wu,[8] J. Wu,[10,11] L. B. Wu,[3,4] S. S. Wu,[14] X. Wu,[5] Z. Q. Xia,[10] H. T. Xu,[14] Z. H. Xu,[10,11] Z. L. Xu,[10] Z. Z. Xu,[3,4] G. F. Xue,[14] H. B. Yang,[13] P. Yang,[13] Y. Q. Yang,[13] H. J. Yao,[13] Y. H. Yu,[13] G. W. Yuan,[10,11] Q. Yuan,[10,11] C. Yue,[10] J. J. Zang,[10,¶] F. Zhang,[8] S. X. Zhang,[13] W. Z. Zhang,[14] Y. Zhang,[10] Y. J. Zhang,[13] Y. L. Zhang,[3,4] Y. P. Zhang,[13] Y. Q. Zhang,[10] Z. Zhang,[10] Z. Y. Zhang,[3,4] C. Zhao,[3,4] H. Y. Zhao,[13] X. F. Zhao,[14] C. Y. Zhou,[14] and Y. Zhu[14]

(DAMPE Collaboration)[**]

[1] *Gran Sasso Science Institute (GSSI), Via Iacobucci 2, I-67100 L'Aquila, Italy*
[2] *Istituto Nazionale di Fisica Nucleare (INFN)–Laboratori Nazionali del Gran Sasso, I-67100 Assergi, L'Aquila, Italy*
[3] *State Key Laboratory of Particle Detection and Electronics, University of Science and Technology of China, Hefei 230026, China*
[4] *Department of Modern Physics, University of Science and Technology of China, Hefei 230026, China*
[5] *Department of Nuclear and Particle Physics, University of Geneva, CH-1211 Geneva, Switzerland*
[6] *Dipartimento di Matematica e Fisica E. De Giorgi, Università del Salento, I-73100 Lecce, Italy*
[7] *Istituto Nazionale di Fisica Nucleare (INFN)–Sezione di Lecce, I-73100 Lecce, Italy*
[8] *Institute of High Energy Physics, Chinese Academy of Sciences, Yuquan Road 19B, Beijing 100049, China*
[9] *University of Chinese Academy of Sciences, Yuquan Road 19A, Beijing 100049, China*
[10] *Key Laboratory of Dark Matter and Space Astronomy, Purple Mountain Observatory, Chinese Academy of Sciences, Nanjing 210023, China*
[11] *School of Astronomy and Space Science, University of Science and Technology of China, Hefei 230026, China*
[12] *Istituto Nazionale di Fisica Nucleare (INFN)–Sezione di Perugia, I-06123 Perugia, Italy*
[13] *Institute of Modern Physics, Chinese Academy of Sciences, Nanchang Road 509, Lanzhou 730000, China*
[14] *National Space Science Center, Chinese Academy of Sciences, Nanertiao 1, Zhongguancun, Haidian district, Beijing 100190, China*
[15] *Istituto Nazionale di Fisica Nucleare (INFN)–Sezione di Bari, I-70125 Bari, Italy*
[16] *Dipartimento di Fisica "M. Merlin" dell'Università e del Politecnico di Bari, I-70126 Bari, Italy*
[17] *Department of Physics and Laboratory for Space Research, the University of Hong Kong, Pok Fu Lam, Hong Kong SAR 999077, China*

(Received 5 January 2021; revised 25 March 2021; accepted 6 April 2021; published 18 May 2021)

The measurement of the energy spectrum of cosmic ray helium nuclei from 70 GeV to 80 TeV using 4.5 years of data recorded by the Dark Matter Particle Explorer (DAMPE) is reported in this work. A hardening of the spectrum is observed at an energy of about 1.3 TeV, similar to previous observations. In addition, a spectral softening at about 34 TeV is revealed for the first time with large statistics and well controlled systematic uncertainties, with an overall significance of $4.3\sigma$. The DAMPE spectral measurements of both cosmic protons and helium nuclei suggest a particle charge dependent softening energy, although with current uncertainties a dependence on the number of nucleons cannot be ruled out.

DOI: 10.1103/PhysRevLett.126.201102

0031-9007/21/126(20)/201102(7)

*Introduction.*—Galactic cosmic rays (GCRs) are energetic particles traveling across the Galaxy as high-energy beams, and are a unique probe to explore the astrophysical particle accelerators and the interstellar medium of the Galaxy [1]. The energy spectrum of GCRs is expected to be a power-law form for energies below the "knee" (at 3–4 PeV) according to the canonical shock acceleration of particles. However, several experiments surprisingly observed changes in the power-law spectral indices $\gamma$ for protons, helium, and heavy nuclei [2–9]. Specifically, the spectra of GCRs become harder by $\Delta\gamma \simeq 0.1 - 0.2$ at kinetic energies (or rigidities) of several hundred $\mathrm{GeV}/n$ (or GV), and become softer again by $\Delta\gamma \simeq -0.3$ at energies of 15–30 TeV (for protons and possibly helium). The deviations from single power law of the spectra motivate extensive investigations for deeper understanding of the acceleration and propagation mechanisms or of new possible GCR sources (e.g., [10]).

Precise measurements of the GCR spectra, particularly for individual species, are mainly from magnetic spectrometers such as the payload for antimatter-matter exploration and light-nuclei astrophysics (PAMELA) and alpha magnetic spectrometer (AMS-02) whose maximum measurable rigidity can reach only few teravolts. Direct measurements at higher energies were mostly done with balloon-borne calorimeter experiments in the past decades, and the uncertainties (both statistical and systematic) are somewhat large, hindering a good understanding of the spectral features above tera-electron-volt energies [2,3,9,11,12].

The Dark Matter Particle Explorer (DAMPE; [13]) is a satellite-borne particle and $\gamma$-ray detector launched on December 17, 2015. It consists of a plastic scintillator detector (PSD) for charge measurement [14,15], a silicon tungsten tracker-converter (STK) for trajectory measurement [16–18], a $\mathrm{Bi_3Ge_4O_{12}}$ electromagnetic calorimeter (BGO) for energy measurement and electron-hadron discrimination [19], and a neutron detector for additional electron-hadron discrimination [20]. DAMPE is expected to significantly improve the measurement precision of GCR spectra up to 100 TeV energies, due to its large acceptance and a good energy resolution (~1.5% for electrons and $\gamma$ rays [21] and ~30% for nuclei [7]). Dedicated calibrations of each subdetector show that the instrument works very stably on-orbit [22]. In this Letter we report the measurements of the helium spectrum with kinetic energies from 70 GeV to 80 TeV using 4.5 years of the DAMPE flight data. Our results give the first precise measurement of the helium spectral structure above TeV energies.

*Monte Carlo simulations.*—Extensive Monte Carlo (MC) simulations were carried out to explore the response to particles in the detector. The results presented in this work are based on the GEANT4 toolkit of version 4.10.5 [23] with the FTFP_BERT physics list for helium nuclei between 10 GeV and 500 TeV. For the higher energies ($> 25\ \mathrm{TeV}/n$) we also tested the EPOS_LHC model via linking the GEANT4 toolkit with the cosmic ray Monte Carlo (CRMC) interface [24], and found that the differences were negligible ($\lesssim 1\%$). The test beam data at 40 $\mathrm{GeV}/n$ and 75 $\mathrm{GeV}/n$ were used to validate the simulation, and we found a good agreement between data and simulation [25]. The simulated events were generated with an isotropic source and an $E^{-1}$ spectrum. During the analysis, the simulation data were reweighted to an $E^{-2.6}$ spectrum, and the systematic uncertainties from different spectral indices were studied. The isotope $^3$He was mixed with the $^4$He sample following the measurements of AMS-02 [26], with an extrapolation at higher energies. For protons we used the GEANT4 FTFP_BERT physics list between 10 GeV and 100 TeV, and the DPMJET3 model via the CRMC-GEANT4 interface between 100 TeV and 1 PeV [7].

To evaluate the impact from the uncertainties of hadronic models, we also performed simulations with the FLUKA version 2011.2x [27], which uses DPMJET3 for nucleus-nucleus interaction above 5 $\mathrm{GeV}/n$. The same analysis procedures based on the two simulation samples were carried out, and the final differences of the energy spectra were taken as systematic uncertainties from the hadronic models [28].

*Event selection.*—In this analysis we used 54 months of the flight data recorded by DAMPE from January 1, 2016 to June 30, 2020. The events when the detector traveled across the south Atlantic anomaly (SAA) region were excluded. After subtracting the instrumental dead time, which is 3.0725 ms per event (~17.2% of the operation time), the on-orbit calibration time (~1.7%), the time between September 9, 2017 and September 13, 2017 when a giant solar flare affected the operation status of the detector [29], and the SAA passage time (~4.9%), we got a total live time of $1.08 \times 10^8$ s, corresponding to 76.2% of the total operation time.

The data were further filtered with the following steps.

*(i) Preselection.*—A sample of good events was selected with a series of preselection criteria. The events passing the high energy trigger (HET) were used in this analysis. The HET requires that the energy depositions in the first three BGO layers are higher than about 13 times the proton minimum ionizing particle (MIP) energy (about 23 MeV in one layer) and in the fourth layer is higher than 2.4 times proton MIP energy [30]. Besides the HET, we further required that the energy deposition in the first two BGO layers was smaller than that in the third and fourth layers. These conditions guarantee that the shower starts in the beginning of the calorimeter and results in a fairly good energy resolution (~28% at 1 TeV and ~34% at 50 TeV). To avoid the geomagnetic rigidity cut-off effect [31], the energy deposition in the first 13 layers of the BGO calorimeter was required to be larger than 20 GeV. In this work, the first 13 layers of the calorimeter were used to measure the event energy in order to minimize the effect of the saturation of readout electronic which is most severe in the last BGO layer due to the high gain of this layer. Finally,

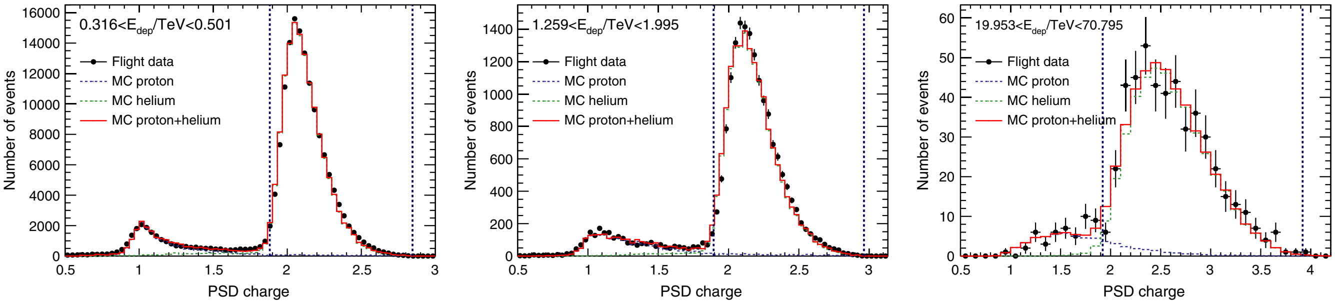

FIG. 1. The distributions of PSD charge, defined as the minimum charge value of the two PSD layers, for events with deposited energy ranges 316–501 GeV (left), 1259–1995 GeV (middle), and 19.95–70.79 TeV (right). The flight data are shown in black points. The histograms show the distributions of the best-fit proton MC (blue), helium MC (green), and proton + helium MC (red). The vertical dashed lines indicate the PSD charge range used to select helium candidate events.

the energy recorded in each layer was required to be less than 35% of the total deposited energy in the first 13 layers. This requirement effectively excludes particles entering from the sides of the detector.

*(ii) STK track selection.*—The number of hits of the reconstructed tracks was required to be $\geq 3$. The track with the maximum total analog-to-digital converter was chosen if there were more than one candidate tracks passing the number of hits selection, and the reduced $\chi^2$ of the track fitting was required to be smaller than 35. Then we required a match between the selected STK track and the reconstructed BGO track, with the following two conditions: (a) the projected distances on each PSD layer for the STK track and the BGO track were smaller than 90 mm, and (b) the average projected distances between the STK track and the centroids of the energy depositions in the first four BGO layers were smaller than 25 mm. Furthermore, to ensure a good shower containment, the reconstructed track was required to be fully contained in the PSD, STK, and BGO subdetectors, and the bar with the maximum energy deposition in each layer was required to be not at the edge of the calorimeter.

*(iii) Charge selection.*—The helium candidates were selected by the charge measured in PSD and STK. The signal of the first hit in the STK track was requested to be higher than 2.5 times the MIP-equivalent signal. This is a very loose STK charge selection to suppress proton events. To properly account for the increase of the energy deposition in the PSD bars with higher particle energies (due to the Bethe-Bloch formula and the backscattering particles), a deposited-energy-dependent selection of the charge reconstructed in both PSD layers ($Y$ layer for the first and $X$ layer for the second),

$$1.85 + 0.02 \log \frac{E_{\mathrm{dep}}}{10\ \mathrm{GeV}} < Z_{X(Y)} < 2.8 + 0.007 \left( \log \frac{E_{\mathrm{dep}}}{10\ \mathrm{GeV}} \right)^{4.0}, \tag{1}$$

was adopted. Note that the energy dependence was not considered in the PSD charge reconstruction [15] algorithm, and the "PSD charge" here was not equivalent to the real particle charge. Finally, the PSD charge reconstructed based on the selected track for both layers was required to be within a factor of 2.

Figure 1 shows the PSD charge (the minimum of $X$ and $Y$ layer measurements [32]) distributions for three selected deposited energy bins, 316–501 GeV, 1259–1995 GeV, and 19.95–70.79 TeV. The vertical dashed lines show the PSD charge selection conditions of Eq. (1). After the STK first-point cut, proton candidates were heavily excluded, which enabled a pure helium sample to be selected in our analysis.

The efficiencies of the selections were obtained from MC simulations. The efficiencies vary with energy, and are about 42%, 84%, and 60% for the preselection, track, and charge selections, respectively, at 1 TeV. For the validations of the main efficiencies one can refer to the Supplemental Material [33]. The effective acceptance after the selection, as a function of the incident energy for incoming helium nuclei, is shown in Fig. 2. Here, the acceptance in the $i$th incident energy bin is computed as

$$A_{\mathrm{eff},i} = A_{\mathrm{gen}} \times \frac{N_{\mathrm{pass},i}}{N_{\mathrm{gen},i}}, \tag{2}$$

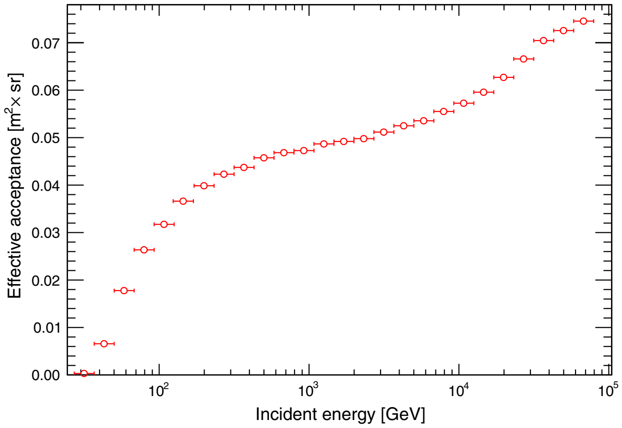

FIG. 2. Effective acceptance after all the analysis selections, as derived from the helium MC sample.

where $A_{\mathrm{gen}}$ is the geometrical factor of the MC event generator sphere, $N_{\mathrm{pass},i}$ refers to the number of events passing the helium selection, and $N_{\mathrm{gen},i}$ is total number of generated events. It is noteworthy that the effective acceptance in this analysis is higher than that of the proton analysis [7], mainly due to the fact that helium events have a higher HET efficiency.

*Background subtraction.*—The main background in helium selection comes from protons. The Landau tail of the proton PSD charge distribution can extend readily to the helium PSD charge window. We employed the MC PSD charge distributions as templates to fit to the data and estimated the background. The template fit was done on the one-dimensional PSD charge distribution of the minimum of $Z_X$ and $Z_Y$. The PSD charge values reconstructed from the MC data and the flight data did not match precisely, especially at high energies, probably due to the back-scattering particles which were not well modeled in the MC simulations. Therefore a smearing of the PSD charge distribution of the MC simulations was applied. The MC templates were shifted and stretched in each deposited energy bin to match with the peaks and widths of the flight data distributions for protons and helium nuclei individually. After the charge smearing, the MC results can well fit the flight data, as shown in Fig. 1. The contaminations of protons were then estimated by counting the number of proton MC events lying in the helium charge window. The proton background varies between ∼0.05% for deposited energy of 20 GeV and ∼4% for 60 TeV. The background fraction in the full energy range is shown in Fig. S5 of the Supplemental Material [33].

*Energy measurements and spectral unfolding.*—In this work we used the first 13 layers of the BGO calorimeter to measure the energy of an event. We also performed two corrections of the energy measurement, as described below. A large energy deposit (approximately above 4 TeV) in a single BGO bar might result in a saturation even of the low-gain readout channel [13,35]. In most cases, the saturation occurred only for a single BGO bar per event. The adoption of 13 layers can effectively exclude the events with multiple saturated bars. We developed a method based on the MC simulations to correct the energy measurements for the saturated events [35]. The other correction was performed in order to account for the Birks' quenching in BGO, which occurred for very low velocity secondary particles [36]. The effect is more significant for heavy nuclei since more secondary particles with large charge and low velocity are produced. We took this effect into account through adding a quenching term in the MC simulations when the ionization energy density was larger than 10 MeV/mm [37]. The quenching effect would result in ∼2% lower deposition of the shower energy for ∼80 GeV incident energy, which translates into ∼5.5% higher helium flux at such an energy after the unfolding. An impact of the quenching effect at different energies is demonstrated in Fig. S6 of the Supplemental Material [33].

An unfolding procedure is necessary to obtain the incident energy spectrum, since only a fraction of the energy of a nucleus can be deposited in the calorimeter. The *observed* number of events $N_{\mathrm{obs},i}$ in the $i$th deposited energy bin is related to the *incident* numbers of events $N_{\mathrm{inc}}$ as

$$N_{\mathrm{obs},i} = \sum_j M_{ij} N_{\mathrm{inc},j}, \tag{3}$$

where $M_{ij}$ is the probability that particles in the $j$th incident energy bin contributing to the $i$th deposited energy bin. The response matrix $M$ for helium nuclei from the GEANT4 FTFP_BERT simulations is given in Fig. S7 of the Supplemental Material [33]. In this work we used the Bayesian unfolding method [38] to derive the incident numbers of events, which were then used to obtain the incident energy spectrum.

*Results.*—The differential helium flux in the incident energy bin $[E_i, E_i + \Delta E_i]$ is given by

$$\Phi(E_i, E_i + \Delta E_i) = \frac{N_{\mathrm{inc},i}}{\Delta E_i A_{\mathrm{eff},i} \Delta t}, \tag{4}$$

where $\Delta E_i$ is the energy bin width, $N_{\mathrm{inc},i}$ is the unfolded number of events, $A_{\mathrm{eff},i}$ is the effective acceptance, and $\Delta t$ is the total live time. The helium spectrum weighted by $E^{2.6}$ in the energy range from 70 GeV to 80 TeV is shown in the top panel of Fig. 3. The error bars show the statistical uncertainties, and the inner and outer shaded bands show the systematic uncertainties from the analysis procedure and the hadronic models, respectively. We also give the fluxes and the associated uncertainties of our measurement in Table S2 of the Supplemental Material [33]. The bottom panel of Fig. 3 shows a comparison of the DAMPE measurement with previous direct measurements by space and balloon-borne detectors [2–4,6,9]. Note that to convert the energy of a helium nucleus to the kinetic energy per nucleon, we assumed an isotope ratio of $^3\mathrm{He}/^4\mathrm{He}$ from the AMS-02 measurements [26]. For the results from other experiments, a pure $^4\mathrm{He}$ sample was usually assumed.

The statistical uncertainties come from the Poisson fluctuations of the number of detected events as well as the MC sample size. Because of the unfolding procedure, the statistical uncertainties cannot be simply translated into the incident energy bins. Following Ref. [7], we generated toy-MC samples based on the numbers of detected events and selected MC events following Poisson distributions in each deposited energy bin, and carried out the spectral unfolding for each simulated observation. The root-mean-square of the final helium fluxes in each incident energy bin is adopted as the statistical uncertainty.

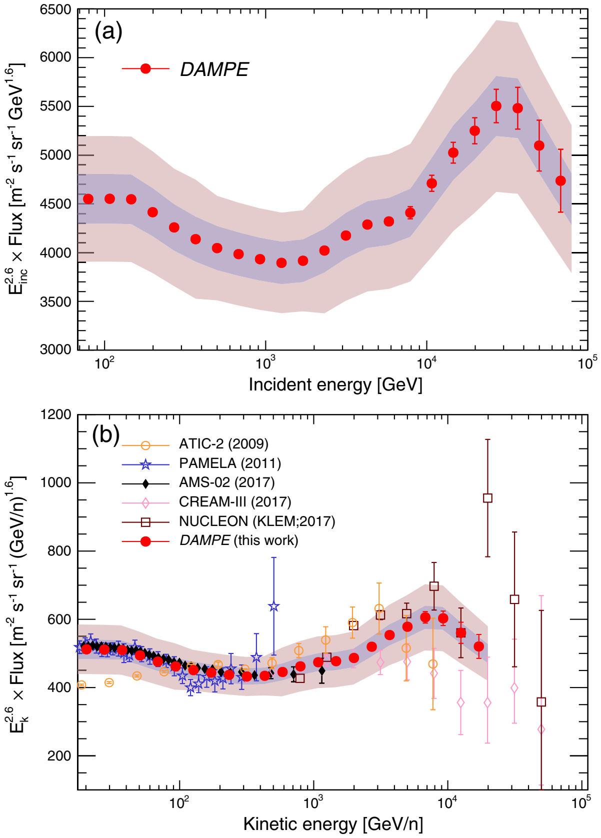

FIG. 3. Helium spectrum weighted by $E^{2.6}$ (top panel) measured by DAMPE. In the bottom panel, we compare the DAMPE spectrum (converted to kinetic energy per nucleon assuming the AMS-02 measured $^3$He/$^4$He isotope ratio [26]) with previous measurements by PAMELA [4], AMS-02 [6], CREAM-III [3], ATIC-2 [2], and NUCLEON (KLEM) [9]. Error bars of the DAMPE data show the statistical uncertainties. The inner and outer shaded bands denote the systematic uncertainties from the analysis ($\sigma_{\rm ana}$) and the total systematic uncertainties including those from hadronic models ($\sqrt{\sigma_{\rm ana}^2 + \sigma_{\rm had}^2}$). For the PAMELA and AMS-02 results, the error bars contain both the statistical and systematic uncertainties added in quadrature. For the other measurements, only the statistical uncertainties are shown.

There are several sources of systematic uncertainties of the measurements. For the event selections, we used the differences between the flight data and the MC simulations for control samples to evaluate the systematic uncertainties. The results turn out to be about ~4% for the HET efficiency ($\sigma_{\rm HET}$), ~0.5% for the track selection efficiency ($\sigma_{\rm track}$), ~3.5% for the charge selection efficiency ($\sigma_{\rm charge}$). We reweighted the spectrum of the MC simulations with spectral index changing from 2.0 to 3.0, and found that the helium fluxes changed by $\lesssim 1\%$. The analysis using energy measurements with 14 layers of the BGO calorimeter led to $\lesssim 1\%$ differences from the results presented here. These two were combined together to give systematic uncertainties from the spectral unfolding, $\sigma_{\rm unf}$. The $^3$He/$^4$He isotope ratio, which mainly affects the calculation of the average number of nucleons, was estimated to contribute to about 0.2% ($\sigma_{\rm iso}$) of the fluxes at low energies (~100 GeV) and even smaller at higher energies via varying the ratio by ±5% which is conservative according to the AMS-02 measurements [26]. We also estimated the effect of background subtraction through varying the PSD charge selection of Eq. (1) by ±5%, and found that the results differed by about 1%–1.5% ($\sigma_{\rm bkg}$). The total systematic uncertainty from the analysis was given by the quadrature sum of the above uncertainties, which was about 5.6%. The absolute energy scale of the measurement, whose uncertainty was estimated to be ~1.3% based on the geomagnetic cutoff of $e^\pm$ [39], would result in a global but tiny shift of the spectrum, and was not included in the total systematic uncertainty. Different analyses obtained consistent results within the uncertainties.

The largest systematic uncertainty comes from the hadronic interaction models. In this work we used the differences between the results based on the GEANT4 and FLUKA simulations as the hadronic model systematic uncertainties, which turned out to be about 12%–15% for incident energies above 300 GeV. At lower energies, we used the test beam data of helium with kinetic energies 40 GeV/$n$ and 75 GeV/$n$ [25] to estimate the efficiencies and energy deposit ratios, and obtained the flux differences between the test beam data and simulation data of ~13%. Thus the systematic uncertainties from the hadronic model below 300 GeV were estimated as 13%. The statistical and systematic uncertainties for different incident energies are summarized in Fig. S8 of the Supplemental Material [33].

From Fig. 3 we can observe that the helium spectrum experiences a hardening at ~TeV energies and then shows a softening around ~30 TeV. The spectral fitting (see the Supplemental Material [33]) gave a significance of the hardening of 24.6$\sigma$, and a hardening energy of $(1.25^{+0.15}_{-0.12})$ TeV. What is more interesting is the softening feature which is clearly shown in the DAMPE spectrum. A possible softening of the spectrum was reported by previous measurements [3,9], but the limited statistics and the large systematic uncertainties prevented a conclusion on this specific point. The significance of the softening from the DAMPE measurements is about 4.3$\sigma$. The softening energy is found to be $34.4^{+6.7}_{-9.8}$ TeV, with a spectral change $\Delta\gamma = -0.51^{+0.18}_{-0.20}$. Together with the softening energy of the DAMPE proton spectrum, $13.6^{+4.1}_{-4.8}$ TeV [7], the results are consistent with a charge-dependent softening energy of protons and helium nuclei, although a mass-dependent softening cannot be excluded by current data.

*Summary.*—The GCR helium spectrum from 70 GeV to 80 TeV is measured with 4.5 years of the DAMPE data. We confirm the hardening feature of the helium spectrum reported by previous experiments. The hardening is smooth with a hardening energy of ~1.3 TeV. The DAMPE data further reveals a softening feature at ~34 TeV with a high significance of 4.3$\sigma$. Combined with the proton spectrum, the softening energy is well consistent with a dependence on particle charge, although a dependence on particle mass can not be ruled out yet. These results will provide important implications in understanding GCR acceleration or propagation processes. Extending the DAMPE measurements to even higher energies is possible with new data and improved analysis performance.

The DAMPE mission was funded by the strategic priority science and technology projects in space science of Chinese Academy of Sciences. In China the data analysis is supported by the National Key Research and Development Program of China (No. 2016YFA0400200), the National Natural Science Foundation of China (No. 11921003, No. 11622327, No. 12003076, No. 11722328, No. 11851305, No. U1738205, No. U1738206, No. U1738207, No. U1738208, No. U1738127), the strategic priority science and technology projects of Chinese Academy of Sciences (No. XDA15051100), the Young Elite Scientists Sponsorship Program by CAST (No. YESS20160196), and the Program for Innovative Talents and Entrepreneur in Jiangsu. In Europe the activities and data analysis are supported by the Swiss National Science Foundation (SNSF), Switzerland, the National Institute for Nuclear Physics (INFN), Italy, and the European Research Council (ERC) under the European Union's Horizon 2020 research and innovation programme (No. 851103).

---

[*] Present address: Gran Sasso Science Institute (GSSI), Via Iacobucci 2, I-67100 L'Aquila, Italy.

[†] Present address: Università di Sassari, Dipartimento di Chimica e Farmacia, I-07100 Sassari, Italy.

[‡] Present address: Università degli Studi di Palermo, Dipartimento di Fisica e Chimica "E. Segrè," via delle Scienze ed. 17, I-90128 Palermo, Italy.

[§] Also at Institute of Physics, Ecole Polytechnique Federale de Lausanne (EPFL), CH-1015 Lausanne, Switzerland.

[‖] Present address: Shandong Institute of Advanced Technology (SDIAT), Jinan, Shandong 250100, China.

[¶] Also at School of Physics and Electronic Engineering, Linyi University, Linyi 276000, China.

[**] dampe@pmo.ac.cn

[1] I. A. Grenier, J. H. Black, and A. W. Strong, Annu. Rev. Astron. Astrophys. **53**, 199 (2015).
[2] A. D. Panov *et al.* (ATIC Collaboration), Bull. Russ. Acad. Sci. Phys. **73**, 564 (2009).
[3] H. S. Ahn *et al.* (CREAM Collaboration), Astrophys. J. Lett. **714**, L89 (2010); Y. S. Yoon *et al.* (CREAM Collaboration), Astrophys. J. **839**, 1 (2017).
[4] O. Adriani *et al.* (PAMELA Collaboration), Science **332**, 69 (2011); Adv. Space Res. **51**, 219 (2013).
[5] M. Aguilar *et al.* (AMS Collaboration), Phys. Rev. Lett. **114**, 171103 (2015); **120**, 021101 (2018); **124**, 211102 (2020).
[6] M. Aguilar *et al.* (AMS Collaboration), Phys. Rev. Lett. **115**, 211101 (2015); **119**, 251101 (2017).
[7] Q. An *et al.* (DAMPE Collaboration), Sci. Adv. **5**, eaax3793 (2019).
[8] O. Adriani *et al.* (CALET Collaboration), Phys. Rev. Lett. **122**, 181102 (2019).
[9] E. Atkin *et al.* (NUCLEON Collaboration), Cosmol. Astropart. Phys. 07 (**2017**) 020.
[10] A. E. Vladimirov, G. Johannesson, I. V. Moskalenko, and T. A. Porter, Astrophys. J. **752**, 68 (2012); P. Blasi, E. Amato, and P. D. Serpico, Phys. Rev. Lett. **109**, 061101 (2012); S. Thoudam and J. R. Hoerandel, Astron. Astrophys. **567**, A33 (2014); P. Lipari, Astropart. Phys. **97**, 197 (2018); C. Yue *et al.*, Front. Phys. **15**, 24601 (2020).
[11] I. P. Ivanenko *et al.*, *23rd International Cosmic Ray Conference*, edited by D. A. Leahy, R. B. Hicks, and D. Venkatesan (World Scientific, Singapore, 1993), Vol. 2, https://ui.adsabs.harvard.edu/abs/1993ICRC....2...17I/abstract.
[12] A. Obermeier, M. Ave, P. Boyle, Ch. Höppner, J. Hörandel, and D. Müller, Astrophys. J. **742**, 14 (2011).
[13] J. Chang *et al.* (DAMPE Collaboration), Astropart. Phys. **95**, 6 (2017).
[14] Y. H. Yu *et al.*, Astropart. Phys. **94**, 1 (2017).
[15] M. Ding *et al.*, Res. Astron. Astrophys. **19**, 47 (2019); T. K. Dong *et al.*, Astropart. Phys. **105**, 31 (2019).
[16] P. Azzarello *et al.*, Nucl. Instrum. Methods Phys. Res., Sect. A **831**, 378 (2016).
[17] A. Tykhonov *et al.*, Nucl. Instrum. Methods Phys. Res., Sect. A **893**, 43 (2018).
[18] X. Li *et al.*, Proc. Sci. ICRC2019 (**2020**) 576.
[19] Z. Zhang *et al.*, Nucl. Instrum. Methods Phys. Res., Sect. A **836**, 98 (2016).
[20] Y. Y. Huang, T. Ma, C. Yue, Y. Zhang, M.-S. Cai, J. Chang, T.-K. Dong, and Y.-Q. Zhang, Res. Astron. Astrophys. **20**, 153 (2020).
[21] G. Ambrosi *et al.* (DAMPE Collaboration), Nature (London) **552**, 63 (2017).
[22] G. Ambrosi *et al.*, Astropart. Phys. **106**, 18 (2019); P. X. Ma *et al.*, Res. Astron. Astrophys. **19**, 082 (2019); A. Tykhonov *et al.*, Nucl. Instrum. Methods Phys. Res., Sect. A **924**, 309 (2019).
[23] S. Agostinelli *et al.*, Nucl. Instrum. Methods Phys. Res., Sect. A **506**, 250 (2003).
[24] CRMC (Cosmic Ray Monte Carlo package); https://web.ikp.kit.edu/rulrich/crmc.html; A. Tykhonov *et al.*, Proc. Sci. ICRC2019 (**2019**) 143.
[25] Y. Wei *et al.*, Nucl. Instrum. Methods Phys. Res., Sect. A **922**, 177 (2019); Y. Zhang *et al.*, Nucl. Instrum. Methods Phys. Res., Sect. A **953**, 163139 (2020).
[26] M. Aguilar *et al.* (AMS Collaboration), Phys. Rev. Lett. **123**, 181102 (2019).
[27] T. T. Bohlen, F. Cerutti, M. P. W. Chin, A. Fassò, A. Ferrari, P. G. Ortega, A. Mairani, P. R. Sala, G. Smirnov, and V. Vlachoudis, Nucl. Data Sheets **120**, 211 (2014).
[28] W. Jiang *et al.*, Chin. Phys. Lett. **37**, 119601 (2020).
[29] https://solarflare.njit.edu/datasources.html.
[30] Y. Q. Zhang, J.-H. Guo, Y. Liu, C.-Q. Feng, Y.-L. Zhang, T.-K. Dong, J.-J. Zang, and C. Yue, Res. Astron. Astrophys. **19**, 123 (2019).
[31] E. Thébault *et al.*, Earth Planets Space **67**, 79 (2015).
[32] Note that we selected events using both charge in the $X$ and $Y$ layers of PSD. However, for the background estimate, the

template fitting algorithm which is described in the text was applied to the one-dimensional PSD charge distribution defined as the minimum of $Z_X$ and $Z_Y$.

[33] See Supplemental Material at http://link.aps.org/supplemental/10.1103/PhysRevLett.126.201102 for efficiency validations, background estimate, energy corrections and response, measured fluxes and systematic uncertainties, and the spectral fitting, which includes Ref. [34].

[34] S. Abdollahi *et al.*, Phys. Rev. D **95**, 082007 (2017).

[35] C. Yue, P.-X. Ma, M. Di Santo, L.-B. Wu, F. Alemanno, P. Bernardini, D. Kyratzis, G.-W. Yuan, Q. Yuan, and Y.-L. Zhang, Nucl. Instrum. Methods Phys. Res., Sect. A **984**, 164645 (2020).

[36] J. B. Birks, Proc. Phys. Soc. London Sect. A **64**, 874 (1951).

[37] Y. F. Wei *et al.*, IEEE Trans. Nucl. Sci. **67**, 939 (2020).

[38] G. D'Agostini, Nucl. Instrum. Methods Phys. Res., Sect. A **362**, 487 (1995).

[39] J. J. Zang *et al.*, Proc. Sci. ICRC2017 (**2017**) 197.